# Strain and phase transformation co-mediated magnetoelectric effect in epitaxial Ni/PMN-PT (011) heterostructures

Yuanzhi Xiang<sup>1</sup>, Peng Zhou<sup>1,†</sup>, Yajun Qi<sup>1</sup>, Kun Liang<sup>1</sup>, Zhijun Ma<sup>1</sup>, Ying Liu<sup>1,2</sup>, Zhuo Yan<sup>1</sup>, Pengcheng Du<sup>1</sup>, Rui Xiong<sup>3</sup>, Yong Liu<sup>3</sup>, Zhengcai Xia<sup>4</sup>, Maksym Popov<sup>2,5</sup>, Dmitry Filippov<sup>6</sup>, Jitao Zhang<sup>7</sup>, Gopalan Srinivasan<sup>2</sup>, and Tianjin Zhang<sup>1,\*</sup>

<sup>1</sup>Key Laboratory of Green Preparation and Application for Materials, Ministry of Education, Hubei Provincial Key Laboratory of Polymers, Department of Materials Science and Engineering, Hubei University, Wuhan 430062, China

<sup>2</sup>Physics Department, Oakland University, Rochester, Michigan 48309, USA

<sup>3</sup>School of Physics and Technology, and the Key Laboratory of Artificial Micro/Nano Structures of Ministry of Education, Wuhan University, Wuhan 430072, China

<sup>4</sup>Wuhan National High Magnetic Field Center & School of Physics, Huazhong University of Science and Technology, Wuhan 430074, China

<sup>5</sup>Faculty of Radiophysics, Electronics and Computer Systems, Taras Shevchenko National University of Kyiv, Kyiv 01601, Ukraine

<sup>6</sup>Novgorod State University, Veliky Novgorod 173003, Russia

<sup>7</sup>College of Electrical and Information Engineering, Zhengzhou University of Light Industry, Zhengzhou 450002, China

<sup>†&</sup>lt;u>p zhou@outlook.com</u> (Peng Zhou)

<sup>\*</sup>zhangtj@hubu.edu.cn (Tianjin Zhang)

## **Abstract**

E-tuning of magnetic behavior is investigated in epitaxial Ni film grown on (011)-PMN-PT single crystal substrate. Loop-like and butterfly-like  $H_r$ -E and  $H_{me}$ -E curves are obtained along [01-1] and [100], respectively, which is mediated by the combined effects of anisotropic strain and nonvolatile rhombohedral to orthorhombic phase transformation in PMN-PT. The results are further confirmed via E-tuning of domain in PMN-PT using piezoelectric force microscope and E-tuning of magnetic stripe domain in Ni film using magnetic force microscope, as well as E-tuning of XRD. In addition, the highest E-induced  $H_r$  shift of 1253 Oe is achieved along [01-1] under electric field of -10 kV/cm. This work is of significance for the potential application in magnetoelectric multifunctional devices.

**Key words:** Magnetic behavior, Anisotropic strain, Phase transformation, Magnetic stripe domain

#### Introduction

Magnetoelectric (ME) composites of ferromagnetic/ferroelectric (FM/FE) heterostructures have attracted intensified interests due to the mutual coupling between ferroic properties and the promising application in next generation reconfigurable RF/microwave communication systems, spintronics devices, magnetic field sensing, etc<sup>[1, 2]</sup>. 0.7Pb(Mg<sub>1/3</sub>Nb<sub>2/3</sub>)O<sub>3</sub>–0.3PbTiO<sub>3</sub> (PMN–PT) single crystal is one of the best candidates used as FE in FM/FE heterostructure because of its ultrahigh piezoelectric response, large anisotropic electric field strain values, and the composition that is near the morphotropic phase boundary (MPB) [3-5]. Under electric field (011)-oriented PMN-PT single crystal allows up to 90% of the ferroelastic domain switching (71° and 109° switching), while (001)-oriented one with only 26% of the ferroelastic domain switching (109° switching), where the ferroelastic domain switching contributes to the lattice strain<sup>[6]</sup>. Therefore, controlling the ME effect in FM/(011)-PMN-PT heterostructure will be more effective.

Researches in terms of ME effect of FM/PMN-PT heterostructures are mainly focused on electric field tuning (E-tuning) of non-volatile magnetic anisotropy and magnetization switching<sup>[7-11]</sup>. In general, the dependence of strain ( $\varepsilon$ ) on electric field shows butterfly-like behavior for PMN-PT, revealing that the process of E-tuning of  $\varepsilon$  as well as ME effect in FM/PMN-PT is volatile. Interestingly, Wu *et al.* have demonstrated  $\varepsilon$ -E can be a loop-like behavior by applying an unipolar electric field, which provides the possibility to control the nonvolatile magnetic behavior in FM/(011)-PMN-PT heterostructures via electric field  $^{[6, 12-15]}$ . On the other hand, E-induced nonvolatile phase transition in (011)-PMN-PT with composition of PT close to MPB happens when the electric field reaches a specific value  $^{[16, 17]}$ , unveiling another mechanism to tune nonvolatile ME effect in FM/(011)-PMN-PT heterostructures. The intrinsic property of PMN-PT with piezoelectric coefficient  $d_{31}$  (along [100] direction, see figure 1(a)) of -1750 pC/N and  $d_{32}$  (along [01-1] direction) of 900 pC/N is helpful for realizing anisotropic manipulation of ME response in FM/(011)-PMN-PT<sup>[18]</sup>. So far, most of the reports about FM layers in FM/PMN-PT heterostructures are polycrystalline or amorphous<sup>[10, 19-22]</sup>, the studies involving epitaxial Ni film and exhibit both loop-like and butterfly-like E-tuning magnetic behaviors are still lacking.

In this work, epitaxial Ni film was grown on (011)-PMN-PT single crystal substrate. E-tuning of both loop-like and butterfly-like magnetic behaviors was obtained along different in-plane

directions, which is attributed to the E-induced volatile strain and nonvolatile rhombohedral to orthorhombic phase transformation in PMN-PT. The results were further confirmed by E-tuning of domain switching in PMN-PT and magnetic stripe domain switching in Ni film, as well as electric field control of X-ray diffraction (XRD) peak shift for both Ni film and PMN-PT. This work provides a route to achieve anisotropic E-tuning of magnetic behaviors in FM/PMN-PT heterostructures.

## **Experiment**

Ni film with thickness of 180 nm was grown on (011)-oriented PMN-PT single crystal substrates by magnetron sputtering with Ar pressure and deposition power of 0.5 Pa and 50 W, respectively, at growth temperature of 500 °C. Then the film was in-situ annealed at 500 °C for 1 h. Subsequently, 40 nm Pt layers were deposited on top of Ni film and the other side of PMN-PT, which were used as electrodes for applying electric field and capping layer for preventing oxidation. The sample structure is shown in figure 1 (a) with the dimension of length × width × thickness = 5 mm × 5 mm × 0.25 mm, where thickness of PMN-PT (011) single crystal substrate is 0.25 mm.

The structural properties were measured by XRD using a Bruker D8 Discover four-circle diffraction system (CuK $\alpha$ 1,  $\lambda$  = 1.5406 Å). Static magnetic property of the heterostructure was performed via superconducting quantum interference device (SQUID). Dynamic magnetic properties were characterized by ferromagnetic resonance (FMR, Bruker, EMX Plus), and magnetic force microscope (MFM) and piezoelectric force microscope (PFM) (Asylum Research MFP-3D Origin). All of the measurements were conducted at room temperature.

#### Results and discussion

Figure 1(b) shows XRD  $\theta$ -2 $\theta$  scan of (011)-oriented Ni/PMN-PT heterostructure, where only (022) diffraction peak is detected, indicating oriented growth for Ni film.  $\phi$ -scan performed on (001) plane exhibits two-fold symmetry, and the film and substrate show diffraction peaks at the same values of  $\phi$ , demonstrating epitaxial growth of Ni film, as shown in figure 1(c). The epitaxial relationship between film and substrate can be written as: Ni (011)[100] || PMN-PT (011)[100].

Static magnetic properties of as-grown Ni film are illustrated in figure 2. Obviously, [01-1] direction is easier to be magnetized than [100] direction in film plane, as indicated in figure 2(a). Angular dependent FMR fields ( $H_r$ ) exhibit a two-fold symmetry with  $H_r$  lower along [01-1] than that along [100], which is in agreement with the structural property shown in figure 1(c) and magnetic property shown in figure 2(a). The experimental data of  $H_r$  vs  $\theta$  can be fitted using formula (1) [23, 24], see figure 2(b),

$$f = \gamma \sqrt{(H_r + 4\pi M_{eff} + (-\frac{3}{8} + 2\cos(2\theta) + \frac{3}{8}\cos(4\theta))\frac{H_4}{2})(H_r + (\frac{1}{2}\cos(2\theta) + \frac{3}{2}\cos(4\theta))\frac{H_4}{2})}$$
(1)

Where resonance frequency f is fixed to 9.85 GHz in this work,  $\gamma$  is gyromagnetic ratio with value of 3.05 GHz/kOe <sup>[25]</sup>,  $H_r$  and  $H_4$  are resonance field and cubic magnetocrystalline anisotropy field, respectively,  $\theta$  is the angle between in-plane magnetic field and [100], and  $M_{\rm eff}$  is effective magnetization.  $M_{\rm eff}$  and  $H_4$  with the values of 0.459 kOe and -0.249 kOe, respectively, are obtained from the fit using formula (1).  $4\pi M_{\rm eff} = 4\pi M_s + H_u$ , where  $4\pi M_s$  and  $H_u$  are saturation magnetization and growth induced uniaxial anisotropy, respectively.  $H_u$  can be calculated as 0.226 kOe based on  $M_s$  obtained from figure 2 (a).

Dynamic magnetic properties were characterized by E-tuning of FMR, where the electric field is scanned from 0 to 10 kV/cm, then to -10 kV/cm, and finally goes back to 0. The relationship between  $H_r$  and E as well as  $H_{me}$  and E along [100] and [01-1] is illustrated in figures 3(a)-(b). Here,  $H_{me}$  is the E-induced anisotropy field, which is determined by formula (2):

$$f = \gamma \sqrt{(H_r + 4\pi M_{eff} + (-\frac{3}{8} + 2\cos(2\theta) + \frac{3}{8}\cos(4\theta))\frac{H_4}{2} + H_{me})(H_r + (\frac{1}{2}\cos(2\theta) + \frac{3}{2}\cos(4\theta))\frac{H_4}{2} + H_{me})}$$
(2)

Specifically, for  $\theta = 0^{\circ}$ ,

$$f = \gamma \sqrt{(H_r + 4\pi M_{eff} + H_4 + H_{me})(H_r + H_4 + H_{me})}$$
 (3)

For  $\theta = 90^{\circ}$ ,

$$f = \gamma \sqrt{(H_r + 4\pi M_{eff} - H_4 + H_{me})(H_r + \frac{1}{2}H_4 + H_{me})}$$
 (4)

Then  $H_{\text{me}}$  can be calculated using formulas (3) and (4) based on  $M_{\text{eff}}$  and  $H_4$  obtained from previous fit.  $H_r$ -E and  $H_{\text{me}}$ -E curves along [100] exhibit butterfly-like (an overlap of butterfly-like and loop-like) behavior, while the curves along [01-1] show loop-like behavior, which is different from the results reported earlier that either show loop-like or butterfly-like E-tuning of magnetic behavior [6]. Electric field control of loop-like magnetic behavior in FM/PMN-PT heterostructures is usually realized by applying a specific unipolar electric field that is high enough to rotate the non-180° (71° and 109°) ferroelastic domain switching [6, 12, 13]. The other method that can be used to induce nonvolatile loop-like behavior is manipulating the rhombohedral to orthorhombic phase transformation in PMN-PT [16, 17]. In current work, we apply bipolar electric field with the field amplitude higher than coercive field, indicating that the loop-like behavior shown in figures 3(a) and (b) doesn't rely on E-induced non-180° ferroelastic domain switching. As a consequence, the loop-like behavior could be the result of phase transformation in PMN-PT.

Figure 4 shows E-tuning of in-plane and out-of-plane domains in PMN-PT using PFM. For the unpoled state, all of the polarization vectors randomly point along eight body diagonals of the pseudocubic cell with rhombohedral symmetry, and the different domain structures (180°, 109°, and 71°) are discernable, as illustrated in figures 4(a), (b), and (g). After applying +6 V (assume positive electric fields point downward), the polarization vectors are switched downward, and the related in-plane and out-of-plane domains are changed also, see figures 4(c), (d), and (h). Further applying -6 V will switch the polarization vectors upward, as shown in figure 4(i). While the in-plane domains are not switched much as compared to the image in figure 4(d), revealing that bipolar electric field doesn't change in-plane ferroelectric or ferroelastic domains, which demonstrates that the loop-like  $H_r$ -E and  $H_{me}$ -E curves in figures 3(a) and (b) are not induced by non-180° ferroelastic domain switching. Nevertheless, however, the out-of-plane domain switching is more significant when flip the external electric field, see figures 4(c) and (e).

The as-grown Ni film has magnetic stripe domain, as shown in MFM image in figure 5(a). Here, magnetic probe detects only the magnetic dipole with magnetization perpendicular to the sample surface [26]. To protect the measurement system, unipolar electric field was applied here. With

applying electric field of 5 kV/cm, some of the domains break or disappear, see figure 5(b). After increasing electric field value to 10 kV/cm, most of the domains disappear, as illustrated in figure 5(c). While part of the domains appears again with the removal of electric field, see figure 5(d). Enlarged MFM images under consecutive electric fields are illustrated in figure 6(a). The related average phase of each MFM image and its variation with electric field are summarized in figure 6(b). Obviously, average phase value decreases quickly after 8 kV/cm, which corresponds to the rhombohedral to orthorhombic phase transformation in PMN-PT<sup>[16, 17]</sup>. This phase transformation is further confirmed via E-tuning of XRD for both Ni film and PMN-PT substrate, as shown in figure 7. (022) diffraction peaks of Ni film and PMN-PT exhibit similar response to electric field, *i.e.*, out-of-plane lattice constant elongates under electric field, and the diffraction peaks and intensity do not come back to original positions after removal of electric field. Therefore, E-induced structural distortion for PMN-PT is a nonvolatile process, which contributes to the loop-like behavior for Ni film shown in figure 3 and is directly related to rhombohedral to orthorhombic phase transformation in PMN-PT.

In addition, (011)-oriented PMN-PT single crystal substrate has compressive strain about -0.27% along [100] and tensile strain about 0.12% along [01-1] <sup>[8, 9]</sup>. The different E-tuning of  $H_r$ -E and  $H_{me}$ -E curves along [100] and [01-1] shown in figure 3 are manipulated by both anisotropic strain and rhombohedral to orthorhombic phase transformation in PMN-PT. Compressive strain plays more important role than that of phase transformation along [100], while the effect of phase transformation along [01-1] is more significant. In this work, E-tuning of strain and phase transformation are responsible for butterfly-like and loop-like behaviors, respectively. Hence, both loop-like and butterfly-like E-tuning of  $H_r$ -E and  $H_{me}$ -E curves are realized along different directions in figure 3.

Finally, E-tuning of  $H_r$  shift along [100] and [01-1] is summarized in figure 3(c). After applying -10 kV/cm along sample thickness, the in-plane magnetic easy axis is switched from [01-1] to [100].  $H_r$  difference ( $\Delta H$ ) between [100] and [01-1] is changed from 815 Oe at unpoled state to 1657 Oe at -10 kV/cm. According to early report [27], theoretical E-tuning of  $H_r$  shift can be calculated using formulas (5) and (6):

$$H_{eff,[100]} = \frac{3\lambda Y}{M_c(1+\nu)} (d_{31} - d_{32})E \quad (5)$$

$$H_{eff,[01\bar{1}]} = \frac{-3\lambda Y}{M_{s}(1+\nu)} (d_{31} - d_{32})E \quad (6)$$

where  $\lambda$  and Y are saturated magnetostriction constant and Young's modulus of Ni film with respective values of -46 ppm and 200 GPa, and v is Poisson's ratio of  $0.33^{[28]}$ . The calculated  $H_{\text{eff}}$ , [100] and  $H_{\text{eff}}$ , [01-1] are -1264 Oe (formula (5)) and 1264 Oe (formula (6)), respectively, under electric field of -10 kV/cm, which is in good agreement with the respective experimental values of -1219 Oe and 1253 Oe.

## Conclusion

In conclusion, E-tuning of magnetic behaviors were carried out in Ni/(011)-PMN-PT heterostructure. Loop-like and butterfly-like  $H_r$ -E and  $H_{me}$ -E curves were obtained along [01-1] and [100], respectively, which is caused by anisotropic strain and nonvolatile rhombohedral to orthorhombic phase transformation in PMN-PT. The results were further confirmed via E-tuning of domain in PMN-PT using PFM and E-tuning of magnetic stripe domain in Ni film using MFM. In addition, the highest E-induced  $H_r$  shift of 1253 Oe was achieved along [01-1] under electric field of -10 kV/cm. This work is of significance for the application in multifunctional magnetoelectric and electronic devices.

## Acknowledgements

The authors would like to thank Furong Qiu and Jiahui Yang of Bruker BBIO, Shanghai, for the help of electric-field tuning of FMR measurements. This work was supported by the National Natural Science Foundation of China (Grants No. 51372074, No. 11574073, No. 51571152, No. 11774270, and No. 11974104). The research at Oakland University was supported by grants from the National Science Foundation, United States (DMR-1808892 and ECCS-1923732).

## References

- [1] N. A. Spaldin and R. Ramesh, Nat. Mater. 18(3): 203-212 (2019)
- [2] N. X. Sun and G. Srinivasan, Spin 02(03): 1240004 (2012)
- [3] Y. Guo, H. Luo, K. Chen, H. Xu, X. Zhang and Z. Yin, J. Appl. Phys. 92(10): 6134 (2002)
- [4] J. B. Li, G. Rao, G. Liu, J. Chen, L. Lu, X. Jing, S. Li and J. Liang, J. Alloy. Compd. 425(1-2): 373-378 (2006)
- [5] P. Zhou, C. Yang, J. Li, X. Liu, Z. Mei, A. Ye, K. Liang, Z. Ma, Y. Qi, X. Yang and T. Zhang, Appl. Phys. Express 10(2): 023201 (2017)
- [6] M. Liu, B. M. Howe, L. Grazulis, K. Mahalingam, T. Nan, N. X. Sun and G. J. Brown, Adv. Mater. 25(35): 4886-4892 (2013)
- [7] J. Wang, D. Pesquera, R. Mansell, S. Van Dijken, R. Cowburn, M. Ghidini and N. Mathur, Appl. Phys. Lett. 114(9): 092401 (2019)
- [8] W. Liang, F. Hu, J. Zhang, H. Kuang, J. Li, J. Xiong, K. Qiao, J. Wang, J. Sun and B. Shen, Nanoscale 11(1): 246-257 (2019)
- [9] P. Li, C. Zhou, C. Cao, W. Wang and C. Jiang, Phys. Chem. Chem. Phys. 20(40): 25854-25860 (2018)
- [10] C. Feng, Y. Liu, H. Huang, Z. Zhu, Y. Yang, Y. Ba, S. Yan, J. Cai, Y. Lu, J. Zhang, S. Zhang and Y. Zhao, ACS Appl. Mater. Interfaces 11(28): 25569-25577 (2019)
- [11] C. Zhou, L. Shen, M. Liu, C. Gao, C. Jia, C. Jiang and D. Xue, Adv. Funct. Mater. 28(20): 1707027 (2018)
- [12] T. Wu, A. Bur, K. Wong, P. Zhao, C. S. Lynch, P. K. Amiri, K. L. Wang and G. P. Carman, Appl. Phys. Lett. 98(26): 262504 (2011)
- [13] T. Wu, A. Bur, P. Zhao, K. P. Mohanchandra, K. Wong, K. L. Wang, C. S. Lynch and G. P. Carman, Appl. Phys. Lett. 98(1): 012504 (2011)
- [14] M. Liu, J. Hoffman, J. Wang, J. Zhang, B. Nelson-Cheeseman and A. Bhattacharya, Sci. Rep.3: 1876 (2013)
- [15] Z. Lai, C. Li, Z. Li, X. Liu, Z. Zhou, W. Mi and M. Liu, J. Mater. Chem. C 7(28): 8537-8545

(2019)

- [16] M. Shanthi and L. Lim, Appl. Phys. Lett. 95(10): 102901 (2009)
- [17] M. Shanthi and L. Lim, J. Appl. Phys. 106(11): 114116 (2009)
- [18] M. Liu, O. Obi, J. Lou, Y. Chen, Z. Cai, S. Stoute, M. Espanol, M. Lew, X. Situ, K. S. Ziemer,V. G. Harris and N. X. Sun, Adv. Funct. Mater. 19(11): 1826-1831 (2009)
- [19] C. Zhou, M. Zhang, C. Feng, M. Xu, S. Wang and C. Jiang, Phys. Chem. Chem. Phys. 21(38): 21438-21444 (2019)
- [20] Y. Ba, Y. Liu, P. Li, L. Wu, J. Unguris, D. T. Pierce, D. Yang, C. Feng, Y. Zhang, H. Wu, D. Li, Y. Chang, J. Zhang, X. Han, J. Cai, C. W. Nan and Y. Zhao, Adv. Funct. Mater. 28 (2018)
- [21] P. Li, Y. Zhao, S. Zhang, A. Chen, D. Li, J. Ma, Y. Liu, D. T. Pierce, J. Unguris, H. G. Piao, H. Zhang, M. Zhu, X. Zhang, X. Han, M. Pan and C. W. Nan, ACS Appl. Mater. Interfaces 9(3): 2642-2649 (2017)
- [22] C. Jia, F. Wang, C. Jiang, J. Berakdar and D. Xue, Sci. Rep. 5: 11111 (2015)
- [23] C. Kittel, Phys. Rev. 73(2): 155-161 (1948)
- [24] P. Zhou, A. V. Singh, Z. Li, M. A. Popov, Y. Liu, D. A. Filippov, T. Zhang, W. Zhang, P. J. Shah, B. M. Howe, M. E. McConney, G. Srinivasan, M. R. Page and A. Gupta, Phys. Rev. Appl. 11(5) (2019)
- [25] P. E. Wigen, G. N. Kakazei, K. Yu. Guslienko, V. Novosad, A. N. Slavin, V. O. Golub, N. A. Lesnik, and Y. Otani, Appl. Phys. Lett. 85(3):443-445 (2004)
- [26] T. Z, P. Dhanapal, B. M. Wang, H. L. Yang, H. C. Xuan, C. Bi, W. G. Wang, and R. W. Li, Appl. Phys. Lett. 114, 232401 (2019)
- [27] M. Liu, O. Obi, Z. Cai, J. Lou, G. Yang, K. S. Ziemer and N. X. Sun, J. Appl. Phys. 107(7): 073916 (2010)
- [28] Y. Tan, K. Liang, Z. Mei, P. Zhou, Y. Liu, Y. Qi, Z. Ma and T. Zhang, Ceram. Int. 44(5): 5564-5568 (2017)

## **Figure Captions**

Figure 1. (a) Schematic diagram of the sample structure, (b) XRD  $\theta$ -2 $\theta$  pattern, (c) XRD  $\phi$ -scan performed about the (001) crystallographic plane of 180 nm (011)-oriented Ni film grown on PMN-PT substrate.

Figure 2. (a) M-H curves of Ni/PMN-PT(011) heterostructures, the inset shows M-H curves along directions of [100] and [01-1], (b) Angular dependent of in-plane FMR field ( $H_r$ ) for Ni/PMN-PT(011) heterostructures, where dots and line are experimental data and corresponding fit, respectively.

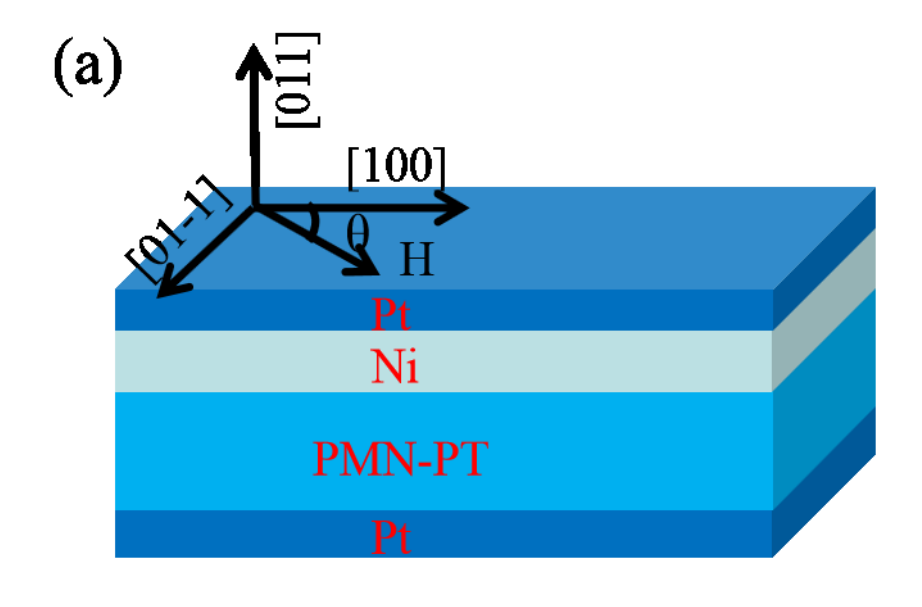
Figure 3 (a)  $H_r$  vs E along [100] (0°) and [01-1] (90°), (b)  $H_{me}$  vs E along [100] and [01-1], and (c) electric-field dependence of  $H_r$  along [100] and [01-1].

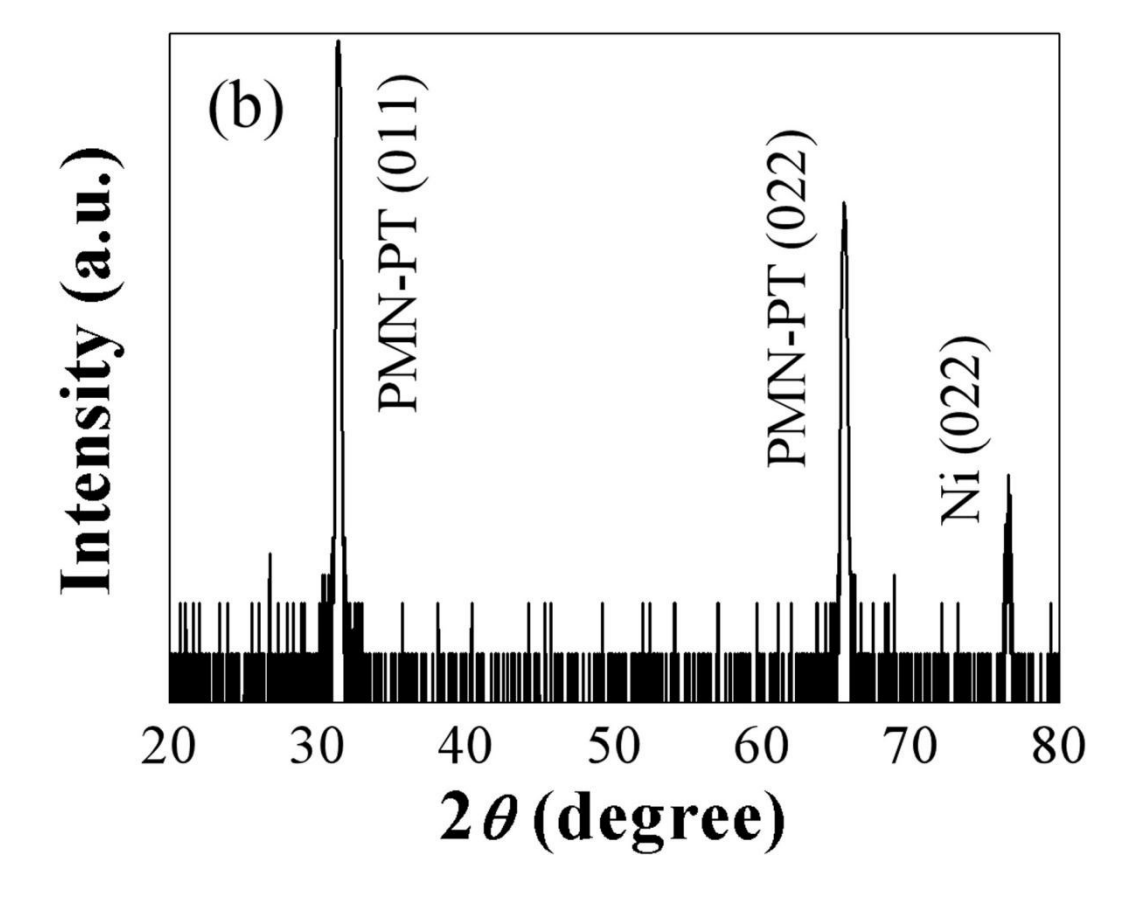
Figure 4. Evolution of in-plane and out-of-plane domains in PMN-PT(011) under electric field of +6 V and -6 V. (a), (c) and (e) are out-of-plane domain images; (b), (d) and (f) are in-plane domain images; (g), (h) and (i) are the sketches of polarization vectors for the unpoled state, under electric field of +6 V and -6 V, respectively. The blue arrows along <111> represent the polarization vectors in the rhombohedral unit cell, and red arrows denote the electric field directions. In (b), (d), and (f), the red hexagon, blue square, and green circle are 109°, 71°, and 180° domains in PMN-PT, respectively.

Figure 5. Stripe domain evolution of Ni film under electric field of 0, 3, 10, and 0' kV/cm, where 0' denotes the state after removal of 10 kV/cm.

Figure 6. (a) Summary of stripe domain evolution of Ni film under various electric field values. (b) Electric field dependent of average phase (unit of milli-degree) of stripe domain.

Figure 7. (a) XRD (022) peak shift of PMN-PT substrate and (b) XRD (022) peak shift of Ni film under electric field of 0, 10 and 0' kV/cm, where 0' denotes the state after removal of 10 kV/cm.





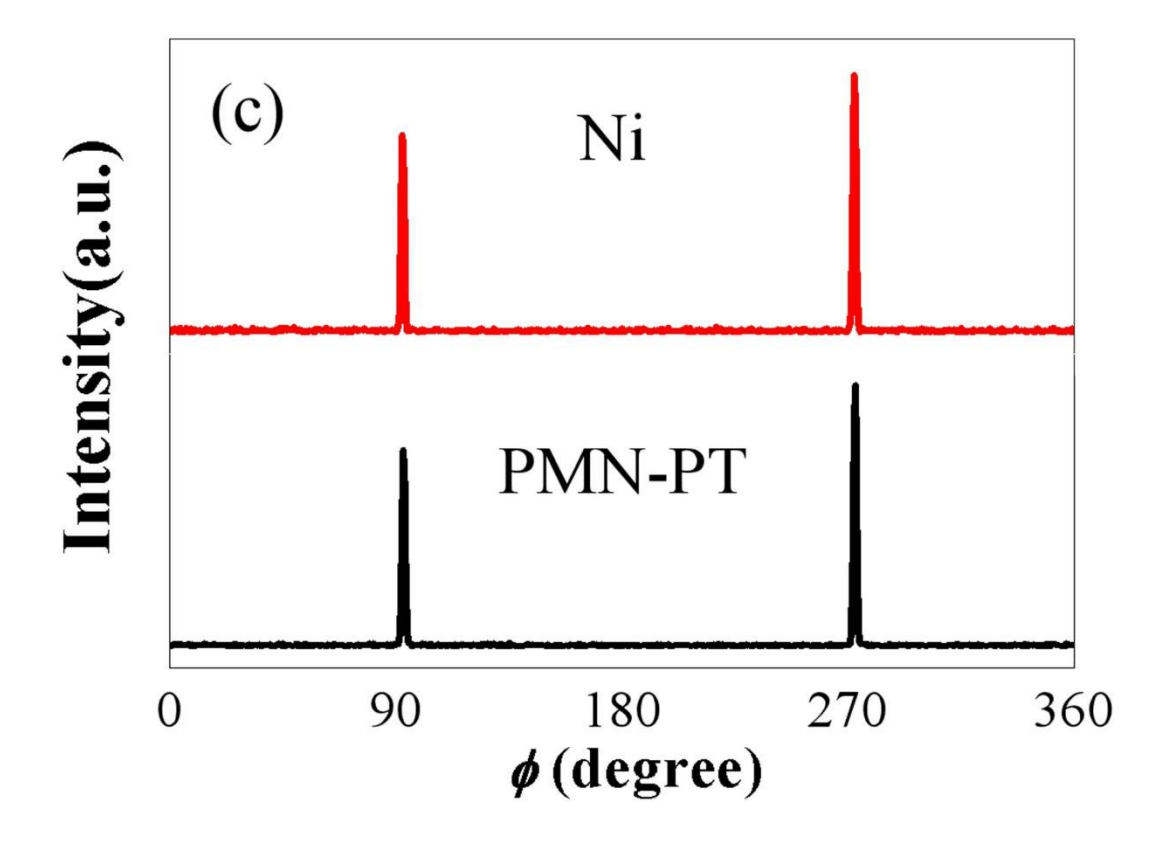
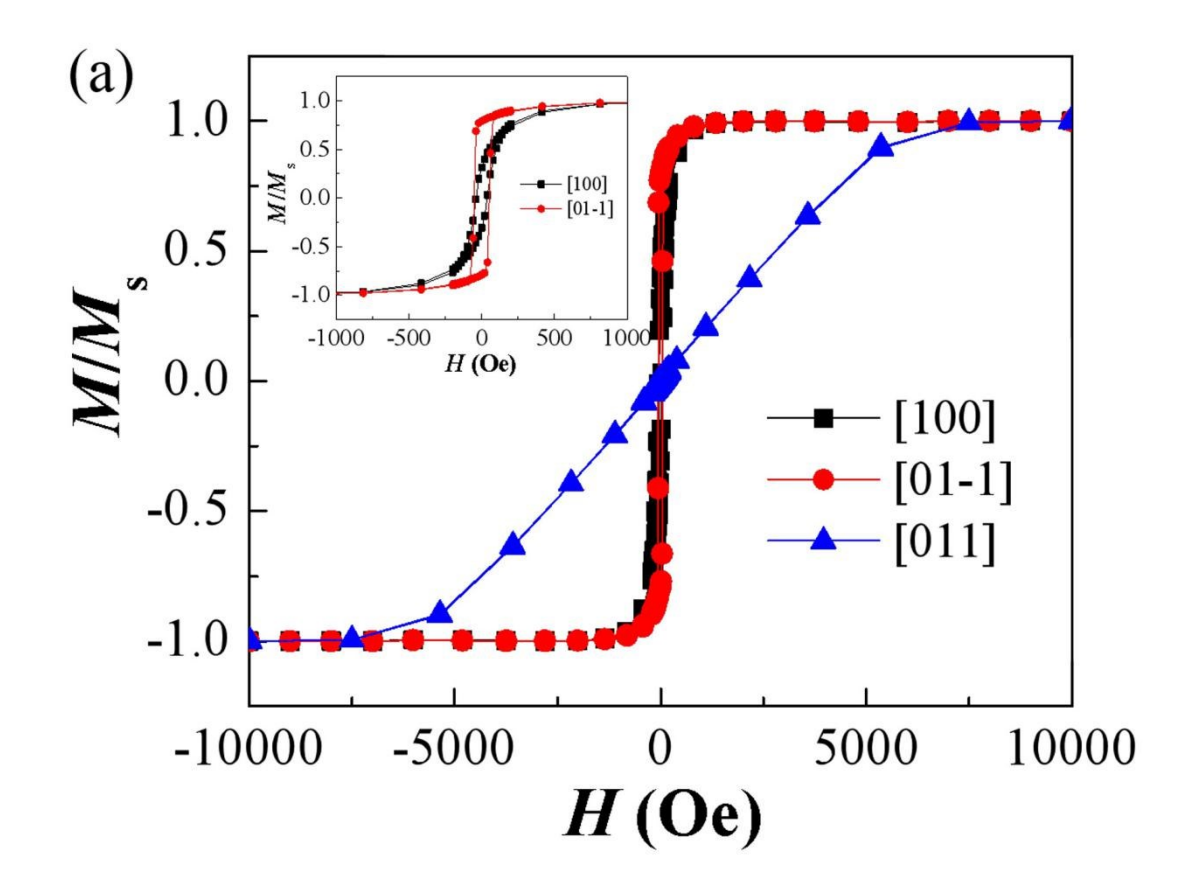


Figure 1



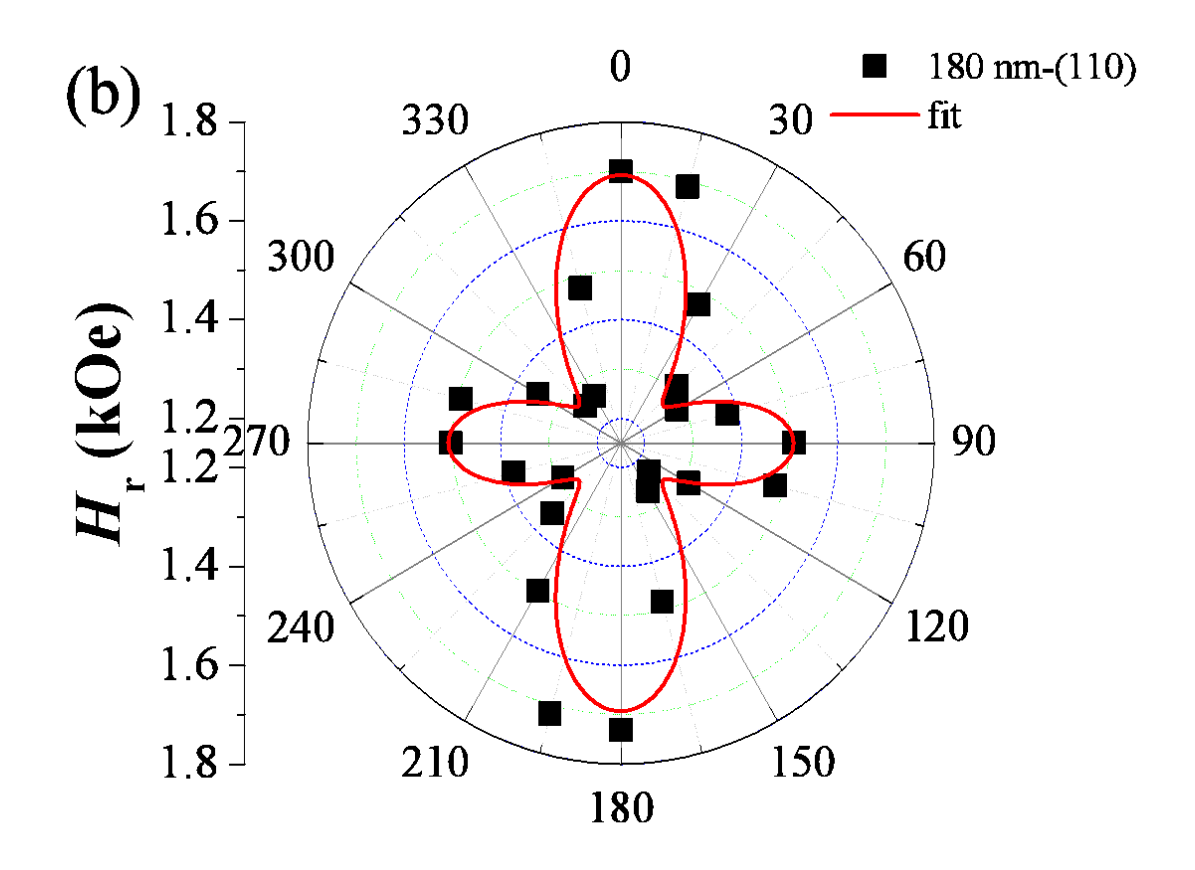
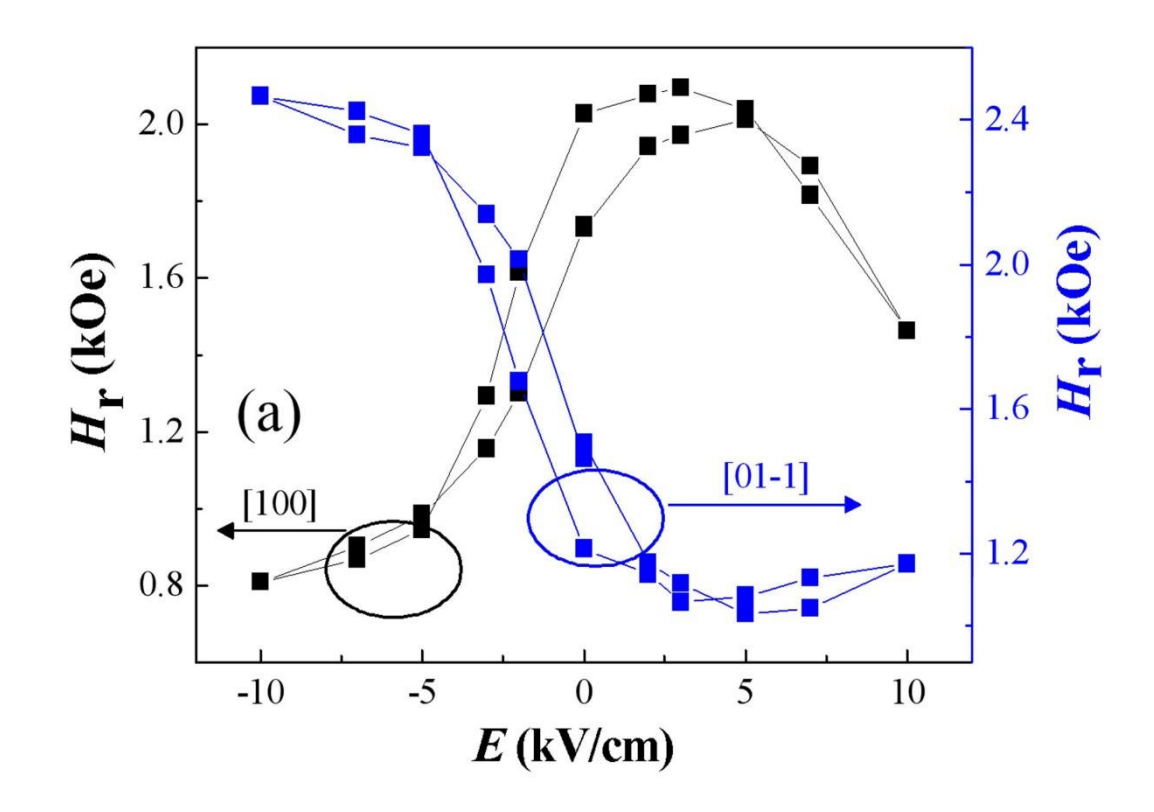
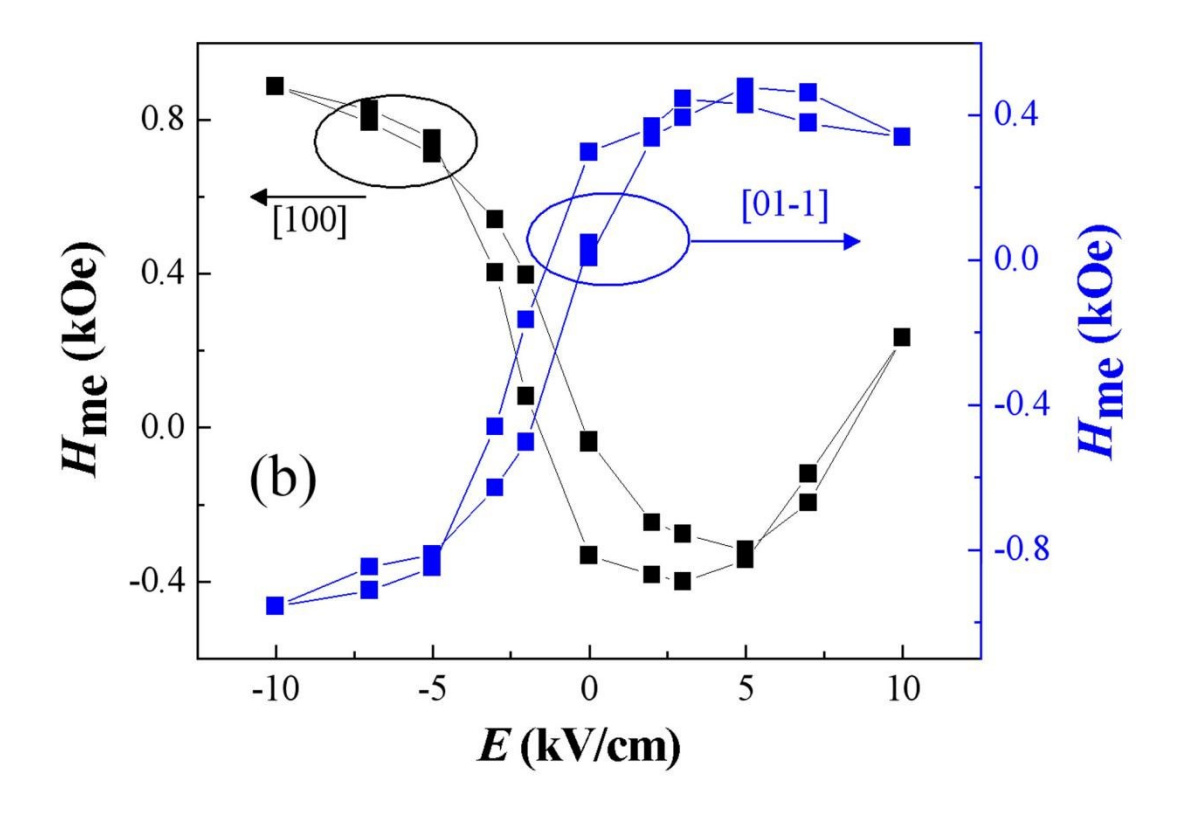


Figure 2





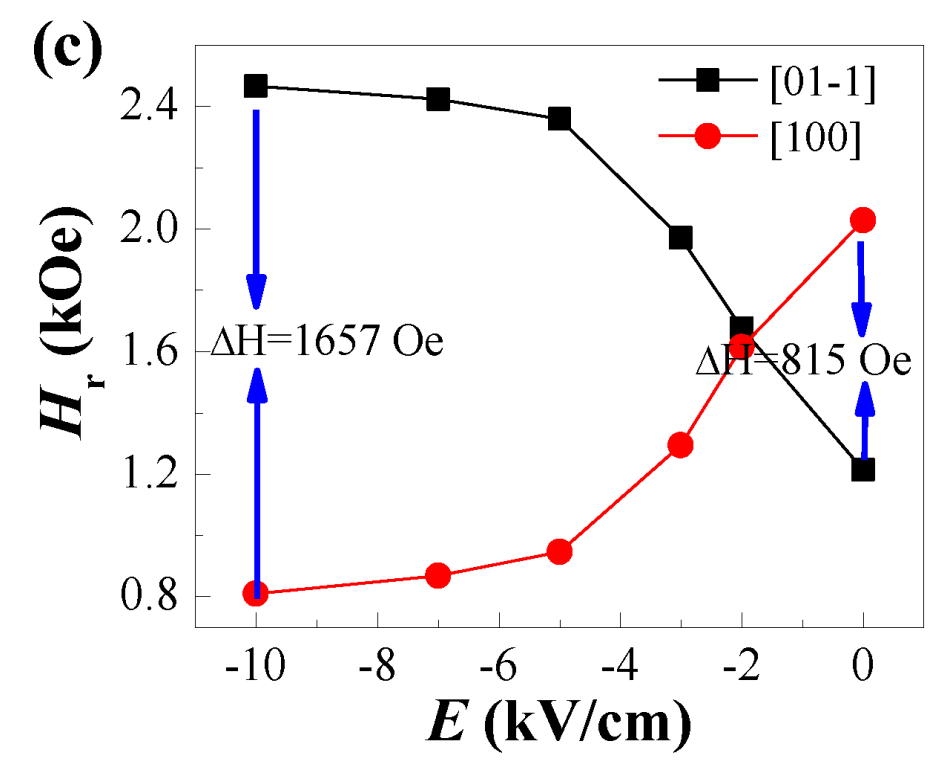


Figure 3

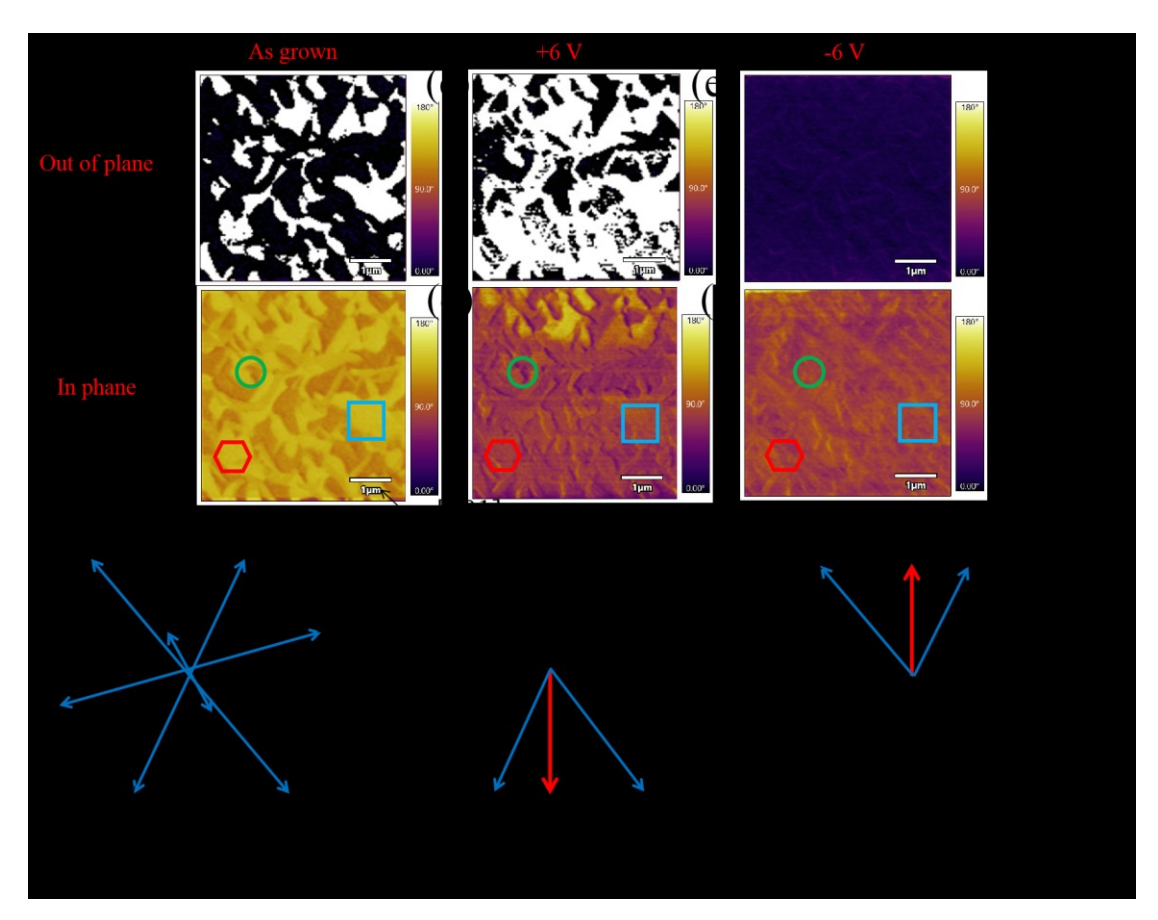


Figure 4

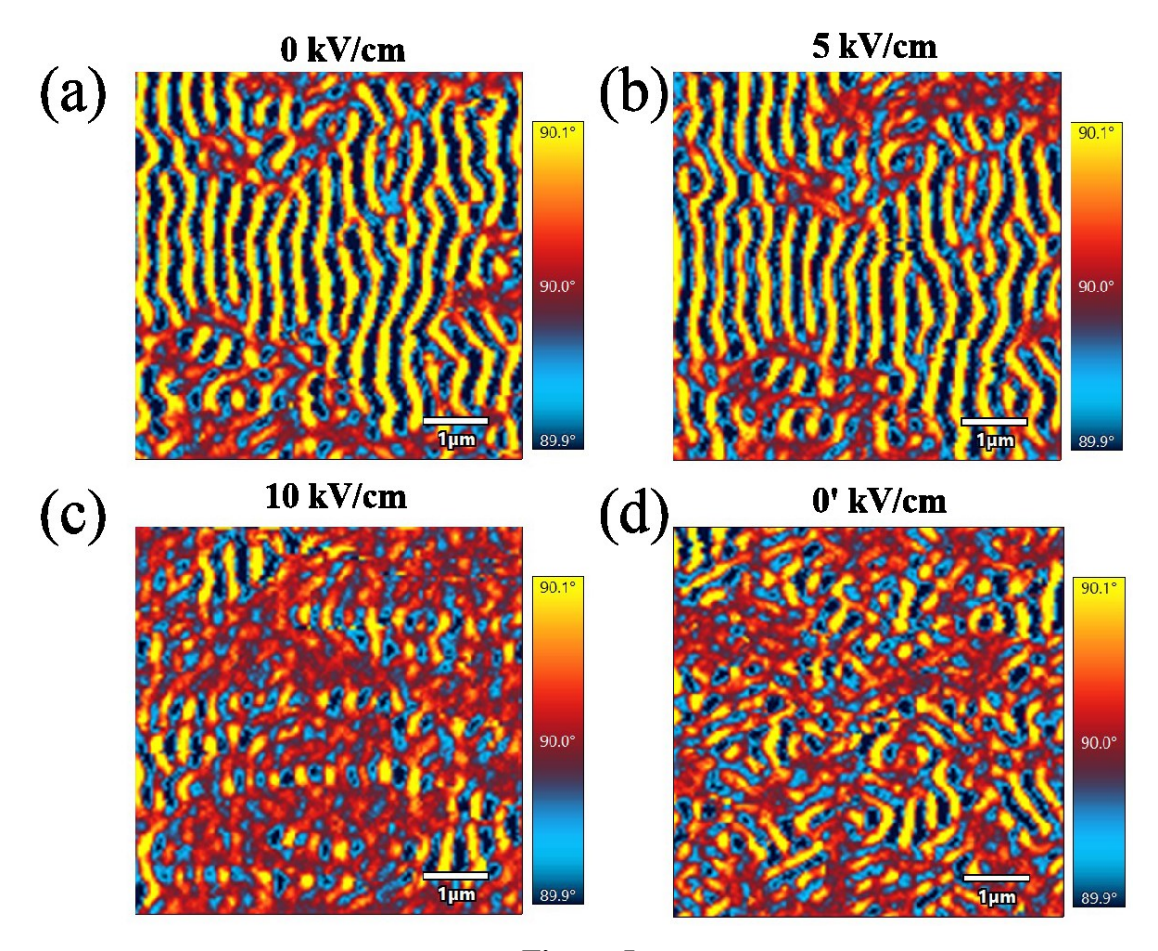


Figure 5

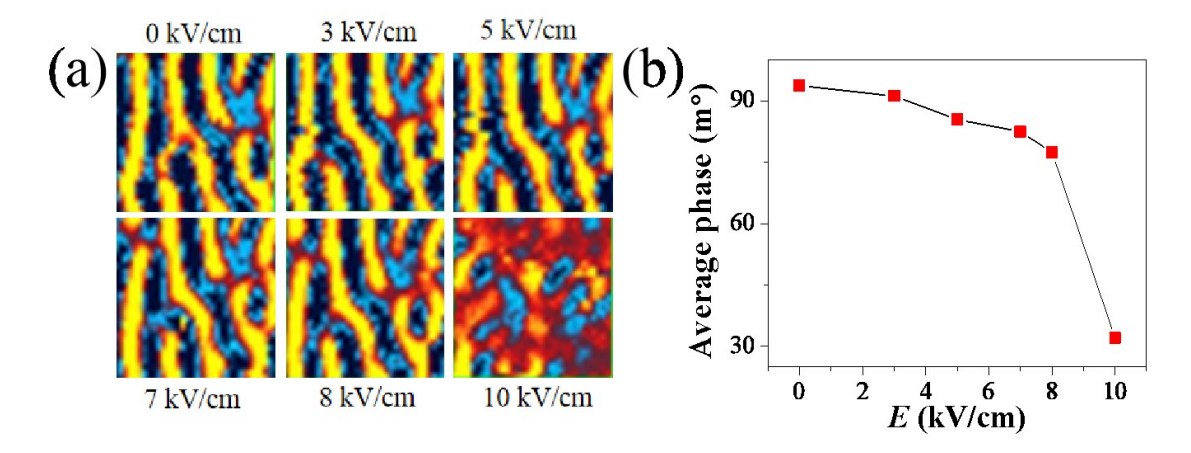
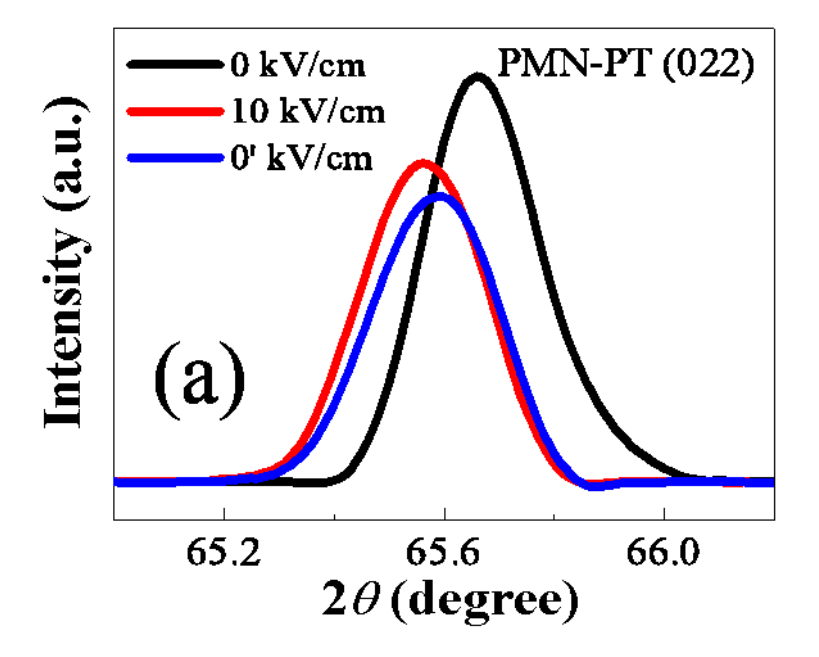


Figure 6



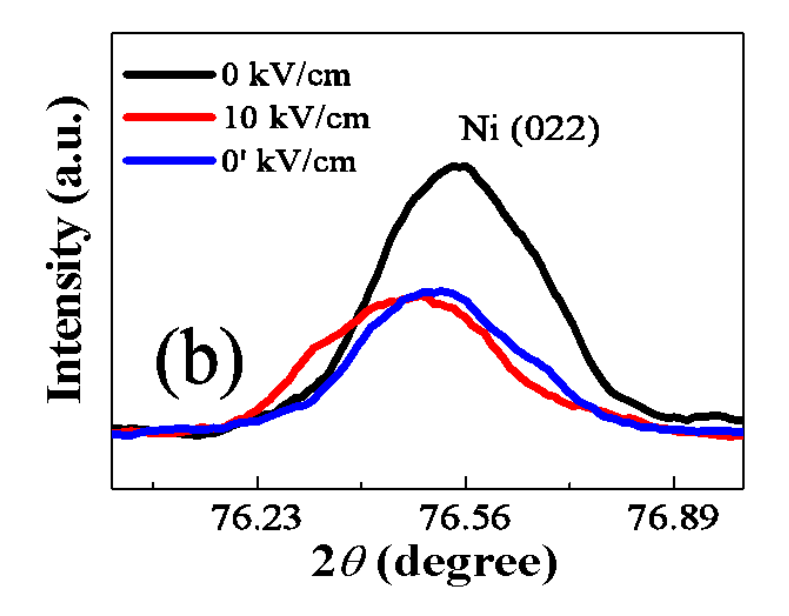


Figure 7